AGU ADVANCING EARTH AND SPACE SCIENCES

Geophysical Research Letters

RESEARCH LETTER
10.1029/2024GL113707

Key Points:

- Coastal upwelling, advection, and plankton dynamics explain variability in surface carbon export by sinking particles
- A Lagrangian growth-advection satellite model performs as well as export derived from ocean color both for surface and abyssal carbon fluxes
- Satellite-derived export products need to consider offsets between production and export, and the role of zooplankton and advection

Supporting Information:

Supporting Information may be found in the online version of this article.

Correspondence to:

M. Messié,
monique@mbari.org

Citation:

Messié, M., Huffard, C. L., Stukel, M. R., & Ruhl, H. A. (2025). Spatial and temporal interplay between oceanic circulation and biological production in shaping carbon export off the California coast. *Geophysical Research Letters*, *52*, e2024GL113707. https://doi.org/10.1029/2024GL113707

Received 18 NOV 2024
Accepted 10 MAR 2025

Spatial and Temporal Interplay Between Oceanic Circulation and Biological Production in Shaping Carbon Export Off the California Coast

M. Messié[1], C. L. Huffard[1], M. R. Stukel[2], and H. A. Ruhl[1]

[1]Monterey Bay Aquarium Research Institute, Moss Landing, CA, USA, [2]Florida State University, Tallahassee, FL, USA

Abstract A major challenge in understanding the oceanic carbon cycle is estimating the sinking flux of organic carbon exiting the sunlit surface ocean, termed carbon export. Existing algorithms derive carbon export from satellite ocean color, but neglect spatiotemporal offsets created by the temporal lag between production and export, and by horizontal advection. Here, we show that a Lagrangian "growth-advection" (GA) satellite-derived product, where plankton succession and export are mapped onto surface oceanic circulation following coastal upwelling, succeeds in representing in situ export off the California coast. In situ export is best represented by a combination of GA export (proportional to modeled zooplankton) and export derived from ocean color (related to local phytoplankton). Both products also correlate with a long-term time series of abyssal carbon flux. These results provide insights on export spatiotemporal patterns and a path toward improving satellite-derived carbon export in the California Current and beyond.

Plain Language Summary Climate on Earth is strongly tied to the carbon cycle, which regulates atmospheric CO_2 concentration. A key component of the oceanic carbon cycle is the downward flux of organic carbon outside of the surface sunlit layer, termed carbon export, which can ultimately sink to the bottom of the ocean and be sequestered for hundreds of years. Direct measurements of carbon export are scarce, so that models and satellite data are needed to understand large-scale patterns. Because organic carbon originates from phytoplankton fixing CO_2 in the ocean surface via photosynthesis, satellite-derived algorithms have been developed by relying primarily on phytoplankton ocean color data. However, such models display poor accuracy. One reason is that they neglect the time elapsed between photosynthesis and carbon export, which can result in a spatial offset of hundreds of kilometers. Our study explicitly considers these offsets and shows that export can also be well represented from space without ocean color, using a plankton model and satellite-derived oceanic currents. These results provide new insights on what controls carbon export, how to represent it from space, and its spatiotemporal patterns in a productive oceanic region.

1. Introduction

The biological carbon pump, which transfers organic matter created by primary production from the surface to the deep ocean, plays a pivotal role in regulating atmospheric CO_2 levels (DeVries, 2022). The gravitational pump, which involves the passive sinking of particulate organic carbon (POC) as dead phytoplankton cells, aggregates, and fecal pellets, is the dominant biological carbon pump pathway globally (Nowicki et al., 2022) and regionally in the California Current Ecosystem (CCE) (Stukel et al., 2023). Its magnitude depends on sinking POC flux at the base of the euphotic zone (carbon export via sinking particles, hereafter "carbon export") and on transfer efficiency in the mesopelagic, which together determine the POC flux to the deep sea and long-term carbon sequestration.

Several algorithms exist that estimate carbon export from remote-sensing data, primarily ocean color. However, considerable unexplained variance remains (Jönsson et al., 2023), even for regionally tuned products (Stukel et al., 2015). Algorithm skill is likely limited by the fact that most are empirical (Brewin et al., 2021) and they often rely on satellite-estimated primary production (itself having non-trivial errors, Siegel et al., 2023). In reality, export is dominated by zooplankton fecal pellets globally (Nowicki et al., 2022) and in productive regions of the CCE (Stukel et al., 2013). One satellite-based mechanistic model considered the role of zooplankton (Siegel et al., 2014) but only performed marginally better than empirical models in the CCE even when tuned regionally (Stukel et al., 2015). One possible explanation is that the method assumed that temporal changes in plankton biomass are exclusively the result of local processes, neglecting horizontal advection. In reality, zooplankton

production is offset in space and time from primary production, particularly in strongly dynamic regions such as CCE (~3 weeks and 50–200 km, Fiechter et al., 2020; Messié & Chavez, 2017; Messié et al., 2022).

Here we assess the potential of a novel satellite-based, Lagrangian "growth-advection" (GA) mechanistic model (Messié et al., 2022), in estimating carbon export from space within the CCE. In the GA model, a simple nutrient, phytoplankton, zooplankton (NPZ) model represents the temporal evolution of plankton communities within surface water masses advected by oceanic currents, following nitrate supply by coastal upwelling. The GA model was originally developed to represent krill hotspots in the CCE (Messié et al., 2022), but also calculates POC production by zooplankton. The only processes included are upwelling, surface advection, and temporal lags created by plankton dynamics. The GA model thus explicitly considers the temporal offset between primary production and carbon export, and the resulting spatial offset due to oceanic advection; it does not rely on satellite-derived primary production or other ocean color products.

This paper compares the satellite-derived GA product to in situ data sets in the central CCE, primarily data from drifting sediment traps deployed by the CCE Long-Term Ecological Research (CCE-LTER) program (Stukel et al., 2023). Carbon export from this data set had been previously related to horizontal advection and water mass age (Chabert et al., 2021), processes that are included in the GA model. Here we take that analysis one step further by also considering nitrate supply at the origin of water mass trajectories (i.e., coastal upwelling) and the corresponding plankton community response including POC production. We first use backward Lagrangian trajectories to demonstrate that in situ export can be reproduced as a function of water mass age and upstream coastal nitrate supply. We then validate the gridded GA export product against in situ export, comparing its performance against another satellite export product based on ocean color (Kahru et al., 2020). Finally, we evaluate the potential of both satellite export products in representing deep-sea POC flux measured at a long-term abyssal time series station (Smith et al., 2018).

2. Materials and Methods

2.1. In Situ and Satellite Data Sets

The CCE-LTER data set includes POC export flux at the base of the euphotic zone off the California central coast (2007–2021) (Stukel et al., 2023, 2024). Sinking POC flux was measured using surface-tethered sediment traps that drifted for 1–7 days over 1–104 km. A power law was used to interpolate or extrapolate to the depth of the euphotic zone (hereafter Zeu) defined as the 0.1% incident light level (Stukel et al., 2024). See Text S1 in Supporting Information S1 for more details.

The Station M time series (Smith et al., 2020) spans 1989–2019 with a few additional dates in 2022 (1993 onward is used here, corresponding with available model estimates). Abyssal POC flux was measured at 3,400 m (600 m above bottom, average location 123°W, 35°N) using a moored sediment trap with rotating collection cups (Baldwin & Glatts, 1998). Each cup collected sinking particles typically for 10 days and the time series was regridded daily by attributing each data point to its corresponding collection duration. An additional 14.5% data points were infilled from a similar trap deployed 50 m above bottom, using a linear relationship between those two traps (Smith et al., 2018).

The analysis relies on several satellite-derived products, including near-surface currents estimated at 15 m depth (GlobCurrent, Rio et al., 2014), nitrate supply by coastal upwelling (hereafter Nsupply, Messié et al., 2022), and a regional product of carbon export derived from ocean color (hereafter EF-OC, based on Kahru et al., 2020). See Text S2 in Supporting Information S1 for details.

2.2. Plankton Model

The NPZ model was originally described by Messié and Chavez (2017); updated equations and parameterization are provided in Figure S1 and Table S1 in Supporting Information S1. POC production within the surface layer ($C_{\text{production}}$, mgC m^{-3} d^{-1}) is set to represent a fixed fraction of excretion by large zooplankton (Z_{big}, tuned to represent krill), such that $C_{\text{production}}$ is proportional to Z_{big}:

$$C_{\text{production}} = \alpha * Z_{\text{big}} \quad (1)$$

When integrated vertically, $C_{\text{production}}$ represents the sinking POC flux at the base of the surface layer (SL) represented by the model. Carbon export at Zeu (C_{Zeu}, mgC m^{-2} d^{-1}) was calculated similarly to sediment trap Zeu export, using the average attenuation coefficient for the CCE-LTER data set (Stukel et al., 2023):

$$C_{\text{Zeu}} = C_{\text{production}} * \text{SL} * e^{-0.72*(\text{Zeu}-\text{SL})/100} \quad (2)$$

SL was set to 30 m, close to typical mixed layers and to the layer represented by GlobCurrent advection (Figure S2 in Supporting Information S1). C_{Zeu} was calibrated against the CCE-LTER data set by tuning the α constant used in Equation 1 (see below), so C_{Zeu} is independent of SL. For comparisons with Station M, a fixed Zeu value of 65.3 m was used, corresponding to the average of CCE-LTER Zeu measured within 100 km of Station M ($N = 8$).

2.3. Backward Analysis of the CCE-LTER Data Set in a Lagrangian Framework

Coastal origin was obtained using 90-day backward trajectories starting from the deployment and recovery positions of each CCE-LTER sediment trap. Trajectories were calculated from GlobCurrent using a 2D custom version of Ariane (Blanke & Raynaud, 1997) used in the GA model (Messié et al., 2022). Each trajectory's coastal origin was defined as the first time the trajectory came within 10 km of the coast (no coastal origin was found for three data points). The 10 km distance is large enough to limit the use of unreliable altimetry and derived currents close to shore and encompass all coastal upwelling (Messié & Chavez, 2015). It is also small enough to reliably estimate water age (offshore currents are ∼5–10 km/day, Messié & Chavez, 2015) and latitudinal origin (given the 25 km Nsupply resolution). Upstream coastal nitrate supply (hereafter source Nsupply) was obtained for each trajectory by interpolating Nsupply at the trajectory's coastal origin in space and time; Nsupply was previously smoothed using a three-point latitude running mean to account for uncertainty in trajectories. Water age was defined as the deployment or recovery time minus the coastal origin time. Sediment traps for which deployment and recovery coastal origins differed by more than 1° latitude or 45 days were excluded from the analysis ($N = 6$); deployment and recovery coastal origin properties were averaged for the remaining sediment traps ($N = 34$). Each sediment trap was matched with output from the NPZ model initialized by its source Nsupply, obtained at the time of its water age. A type-2 linear regression between observed and modeled carbon export was used to calibrate α (Equation 1).

2.4. Satellite-Derived Lagrangian Growth-Advection (GA) Model

The GA model is described in detail by Messié et al. (2022) and only briefly summarized here. The method maps the NPZ model output, including $C_{\text{production}}$, onto 60-day forward surface Lagrangian trajectories originating daily at the coast every 3 km in latitude (28–48°N). The NPZ model was initialized by Nsupply interpolated in time and latitude at each trajectory origin. The trajectories were calculated using an interpolated GlobCurrent product where nearshore gaps were filled at each latitude by using the first available data point, keeping its along-shore component and linearly interpolating its cross-shore component down to 0 at the coast (Messié et al., 2022). Daily Lagrangian runs were combined into daily, then monthly maps at 1/8° resolution (∼12 km).

3. Results

3.1. Along-Trajectory Analysis of the CCE-LTER Sediment Trap Data Set

The backward analysis revealed a clear relationship between Zeu export and source water characteristics (Figure 1). In situ Zeu export was significantly proportional to source Nsupply ($R^2 = 0.28$, $p < 0.01$) and peaked ∼3 weeks after upwelling (Figure 1b). These characteristics are shared by Z_{big} in the NPZ model (Figure 1c; Messié et al., 2022), thus by $C_{\text{production}}$ and C_{Zeu} (Equations 1 and 2). In situ Zeu export was also higher for shallower Zeu (Figure 1b), as represented in Equation 2.

Modeled export C_{Zeu} was compared to, and calibrated with, in situ Zeu export (Figure 2a). The relationship was used to determine $\alpha = 1.75$ gC molC^{-1} d^{-1}, used to scale $C_{\text{production}}$ and C_{Zeu} hereafter. Independent of calibration, the result yields a very good predictive relationship when excluding the 3 traps where Zeu was shallower than 30 m ($R^2 = 0.69$, Table 1). The model performed as well as a relationship based on coincident in situ primary production and temperature ($R^2 = 0.67$, Stukel et al., 2023), even though it did not include any in situ data beyond climatologies. The lack of skill when the euphotic zone was shallow likely occurs because Lagrangian trajectories

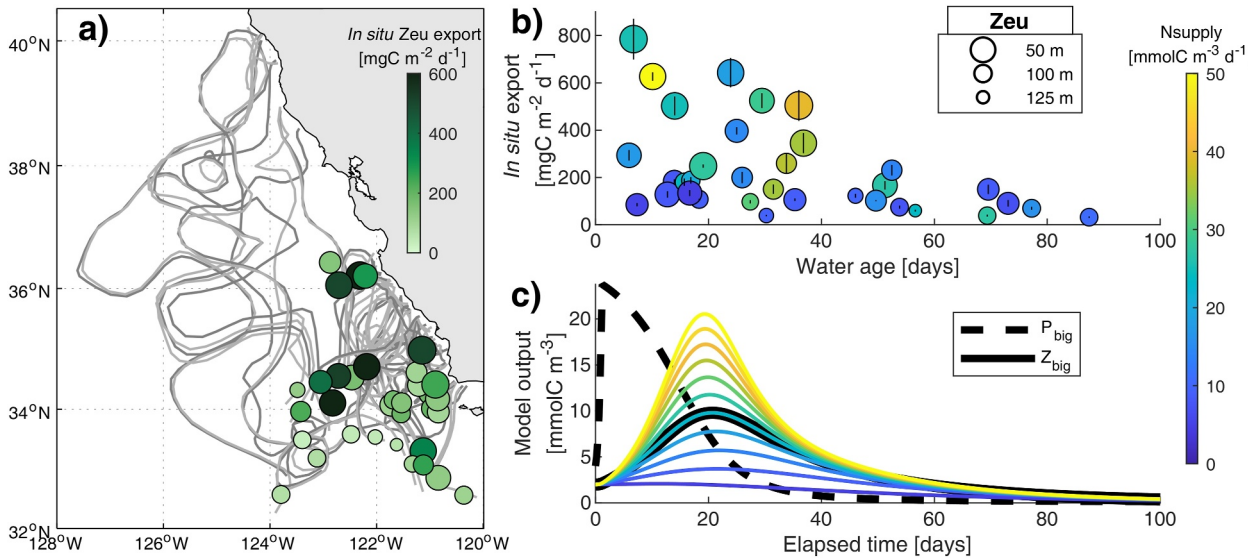

Figure 1. Relationship between Zeu export and coastal origin properties. (a) CCE-LTER sediment trap Zeu export (green dots, position averaging deployment and recovery) with backward trajectories from deployment (dark gray) and recovery (light gray) positions underlaid. Sediment traps where trajectories diverged too much or no coastal origin was identified (see text) are not displayed. (b) In situ Zeu export (*y*-axis, lines represent standard error) as a function of water age (*x*-axis) and source Nsupply (colors). Dot size in a and b is inversely proportional to Zeu. (c) Output from the NPZ model initialized by Nsupply, where thick black lines display large phytoplankton (P_{big}) and large zooplankton (Z_{big}) for an initial Nsupply of 20 mmolC m^{-3} d^{-1}, while colored lines display Z_{big} for a range of initial Nsupply values.

are representative of the top 30–50 m (Figure S2b in Supporting Information S1), and thus do not correctly represent advection above shallower depths.

3.2. Validation of Satellite-Derived Export Against the CCE-LTER Data Set

We compared in situ Zeu export to gridded satellite-derived products by averaging daily EF-OC export and GA $C_{production}$ in time and space between recovery and deployment times and locations. Two sediment traps where the drift was <2 km were excluded (not representative of lower-resolution gridded products, especially 12-km GA);

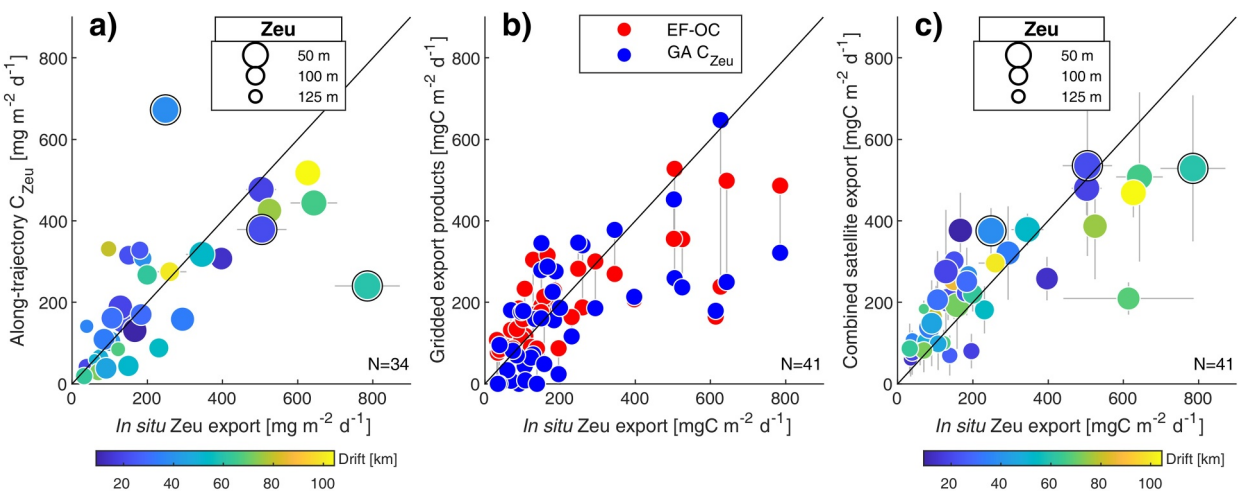

Figure 2. Validation of satellite-derived carbon export products (*y*-axis) against in situ Zeu export (CCE-LTER data set, *x*-axis). (a) Along-trajectory C_{Zeu} predicted at t = water age by the NPZ model initialized by source Nsupply. (b) EF-OC (red) and GA C_{Zeu} (blue) gridded satellite products; gray lines join predictions for the same sediment trap data point. (c) Combined product, calculated as 0.8041*EF + 0.4281*C_{Zeu} (coefficients were determined using a multilinear regression, see text). In a and c, dots are colored as a function of drift between deployment and recovery and dot size is inversely related to Zeu (black circles indicate Zeu < 30 m); gray lines represent standard error.

Table 1
Statistics Comparing Satellite-Derived Products to In Situ Data Sets

Comparison with CCE-LTER Zeu export	N	R^2	log10 R^2	RMSE [mgC m^{-2} d^{-1}]
Along-trajectory backward analysis				
C_{Zeu}	34	0.43	0.57	150
idem where Zeu is below 30 m	31	0.69	0.59	94
Gridded satellite-derived products				
GA C_{Zeu}	41	0.43	0.34	155
EF-OC	41	0.58	0.60	130
Combined product	41	0.66	0.66	114
Comparison with station M POC flux time series at 3,400 m	**Lagged R^2 (daily)**	**Lag [days]**	**R^2 (monthly)**	**R^2 (yearly)**
Gridded satellite-derived products (50-km radius circle around Station M)				
GA C_{Zeu} (fixed Zeu = 65.3 m)	0.18	7	0.20	0.31 ($p < 0.01$)
EF-OC	0.16	4	0.18	$p > 0.05$
Combined product	0.22	6	0.24	0.32 ($p < 0.05$)

Note. N is the number of data points, R^2 the correlation coefficient squared (all correlations are significant at $p < 0.001$ except where indicated, log10 indicates correlation on log10-transformed data), and RMSE the root mean squared error. Correlations with CCE-LTER sediment traps are partly driven by Zeu but remain high after normalizing to 100 m depth (Table S2 in Supporting Information S1). Note that GA RMSEs are improved by α calibration, but correlations are independent of calibration. *P*-values were corrected for autocorrelation in time series comparisons following Pyper and Peterman (1998).

remaining traps drifted for >9 km. GA export (i.e., C_{Zeu}) was estimated for each trap from gridded $C_{production}$ following Equation 2. The correlation between gridded GA C_{Zeu} and in situ export is significantly lower than when calculated along trajectories (Table 1), with GA explaining 43% of the in situ variance as a gridded product (Figure 2b blue) versus 69% along trajectories when excluding shallow Zeu (Figure 2a). This difference is primarily explained by the fact that the gridded GA product is based on forward instead of backward Lagrangian trajectories, so that grid cells include several water mass histories beyond the ones estimated for the deployment and recovery locations. EF-OC performed better (58% variance explained, Figure 2b red), noting that its spatial resolution is higher (4 vs. 12 km).

We combined both satellite products using a multilinear regression against in situ Zeu export (Figure 2c), which represents coastal water parcels advected long distances (GA) interacting and mixing with other nearby water parcels (EF-OC). Despite GA and EF-OC being correlated with each other for the CCE-LTER data set ($R^2 = 0.29$, $p < 0.001$), the combined product still displayed higher accuracy than either product when compared to CCE-LTER sediment traps (66% variance explained, Table 1). Interestingly, GA, EF-OC, and combined products all underestimate high export (>400 mgC m^{-2} d^{-1}, Figures 2b and 2c).

3.3. Comparing Satellite-Derived Surface Export and Abyssal POC Flux

Deep-sea POC fluxes measured at Station M were compared to surface carbon export using time-lagged correlations (Figure 3, Table 1). Correlations were maximal near Station M, within up to ~50–100 km, for both GA and EF-OC products (Figure 3c). POC pulses at 3,400 m often corresponded to peaks in surface export above Station M for both products (Figure 3a). The GA product displays more intense export peaks than EF-OC, generated by a combination of upwelling variability and surface current convergence, and higher variability that more accurately matches the observed variability in deep-sea POC fluxes (Figure 3b). However, there is little overall correspondence between surface (from either product) and deep-sea POC pulse timing and magnitude (Figure 3a). Correlations are significant but low for daily time series although low-frequency variability is better represented (Table 1). Lags were below the 10-day effective resolution of the Station M time series. The combined product performed better than GA or EF-OC alone, explaining ~20–30% of event-scale to interannual variance (Table 1).

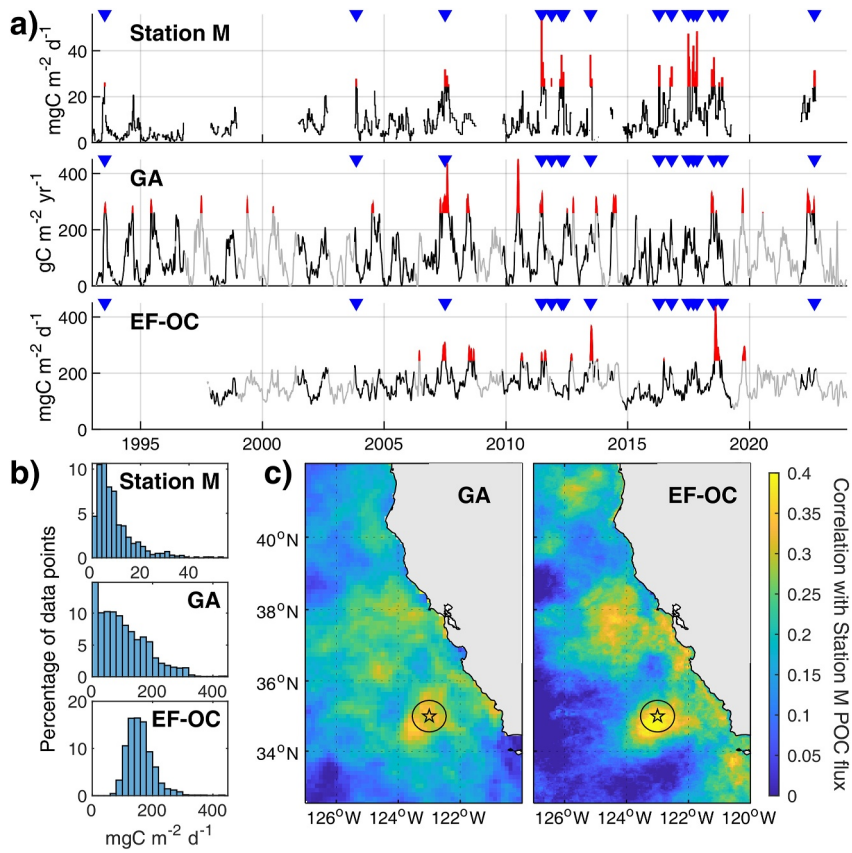

Figure 3. Relationship between satellite-derived carbon export and deep-sea POC flux at Station M. (a) Time series of abyssal POC flux and surface export averaged in a 50-km radius circle. Red indicates pulse events for each time series (defined as exceeding mean +2 standard deviations); blue triangles mark Station M pulse events. Time periods when no Station M data is available are displayed in gray. (b) Time series histograms (the *x*-axis in b corresponds to the *y*-axis in a). (c) Maximum lagged correlation between Station M POC flux at 3,400 m and satellite-derived export at each grid cell. Station M is indicated by a star; the 50-km radius circle is displayed in black. GA low spatial autocorrelation (Figure S3 in Supporting Information S1) explains that correlations can be higher for GA than EF-OC when averaged spatially (Table 1) despite higher per-pixel correlations for EF-OC.

4. Discussion

4.1. GA Export Limitations and Potential for Improvement

The GA model performed very well in predicting in situ POC fluxes, including both abyssal POC flux (relative to EF-OC) and surface export. This is particularly remarkable considering the small set of processes represented (discussed in Text S3 in Supporting Information S1) and the fact that the model was tuned to represent krill hotspots rather than export. Comparisons with Station M point toward a timing issue within the model, however, that offers the strongest potential for improvement. Maximum correlations between Station M and GA export (Figure 3c), representing the mean source location, are found ~50–100 km southwest (downstream) of Station M instead of <50 km as observed for EF-OC and in a model (Ruhl et al., 2020, their Figure 6c). This suggests that export peaked too late in space and/or in time in the GA model, which could also explain unrealistically short lags between surface GA and Station M POC flux (Table 1). Indeed, lags <10 days correspond to average sinking velocities >330 m d^{-1}, which is much higher than identified previously at Station M (averaging 34–137 m d^{-1} overall, 234 m d^{-1} during pulse events, Smith et al., 2008, 2018) and elsewhere (e.g., Picard et al., 2024).

Improving the timing of export in the GA model is beyond the scope of this paper but can be attained by better constraining several aspects, starting with the plankton model. How export is modeled, and its timing following upwelling, can be improved by (a) taking into account the contribution of sinking phytoplankton, (b) improving the zooplankton contribution (e.g., by calculating POC production as a function of zooplankton grazing rather

than biomass), and (c) tuning the model parameters, although it may be challenging to improve the excellent along-trajectory relationship further (Figure 2a).

Tuning timing in the plankton model is, however, complicated by its convolution with timing within Lagrangian trajectories, themselves dependent on satellite-derived currents. The GA method relies on a satellite current product using classical nadir altimetry, which is relatively coarse resolution and subject to caution within 50 km of shore (Bouffard et al., 2008). The newly launched SWOT satellite may improve satellite-derived currents, in particular nearshore where current speed and direction have a disproportionate impact on subsequent current trajectory and timing. As new satellite-derived currents incorporating SWOT data become available, the GA method is likely to become more precise in space and time.

4.2. Processes Driving Carbon Export and Abyssal POC Flux

Models and observations have shown that coastal upwelling drives ecosystem processes in the CCE, including phytoplankton (Fiechter et al., 2018; Messié & Chavez, 2015), zooplankton (Fiechter et al., 2020; Messié et al., 2022), and higher trophic levels down to the abyssal seafloor (Messié et al., 2023). Here, we showed how the interplay of coastal upwelling, oceanic advection, and plankton dynamics also shapes carbon export and abyssal POC flux. Our results indicate that export in the CCE may be best estimated from space by combining local processes assessed from ocean color and lagged processes as derived from the GA model, which yield very different patterns (Figure S4 in Supporting Information S1). The spatial and temporal offset between nutrient supply and fast-growing phytoplankton on one side (tightly coupled in the NPZ model), and slow-growing zooplankton and export on the other side, appears to be crucially important in shaping carbon export in the CCE and needs to be taken into account in satellite-derived export products. Such offset had been highlighted previously in the CCE (e.g., Chabert et al., 2021; Chavez & Messié, 2009; Kranz et al., 2020; Pennington et al., 2009; Plattner et al., 2005; Stukel et al., 2023) but had not yet, to our knowledge, been incorporated into algorithms used to derive export from space.

Deep-sea POC flux measured at Station M had been previously shown to correlate with carbon export derived from ocean color averaged in 50- or 100-km circles above (e.g., Smith et al., 2008, 2018). Comparisons with EF-OC and GA yield similar results, with a mean surface catchment area likely located within 50–100 km above Station M (Figure 3c), although Station M catchment area is variable and can extend much further (Ruhl et al., 2020). Lags are however unrealistically short (see Section 4.1); this suggests timing needs to be improved for GA and perhaps for EF-OC, which integrates primary production during the previous 5 days (no integration in past studies; e.g., Smith et al., 2018).

Interestingly, GA performed better than EF-OC against abyssal POC flux, while EF-OC performed better than GA against Zeu export (Table 1). This likely arises because uncertainty in satellite-derived currents leads to spatial inaccuracies in the GA product that are more pronounced when compared to shallower sediment traps with a smaller catchment area. The GA approach was also able to much more accurately represent the histogram of abyssal POC flux than EF-OC (Figure 3b), which highlights the mechanistic role of zooplankton-mediated lag times and mesoscale advection in driving gravitational flux patterns. Indeed, GA and EF-OC represent different origins of export flux: GA represents the contribution of upstream coastal phytoplankton such as diatoms (via zooplankton fecal pellets) while EF-OC represents the contribution of local phytoplankton (mostly picoplankton offshore). These differences may lead to distinct export characteristics in terms of nature and size of sinking particles and their associated microbial community (e.g., Durkin et al., 2022). Export flux composition further impacts attenuation processes within the ocean mesopelagic zone (Stephens et al., 2024), sinking velocities and thus lags between surface and abyss (Cram et al., 2018), and has been linked to Station M pulse events (Michaud et al., 2022). While carbon export and abyssal POC flux are better represented by combining EF-OC and GA products, considering them separately may thus provide the best value as the fate of the flux they represent may differ.

5. Conclusion

This study used a Lagrangian framework to investigate carbon export, demonstrating the role of upstream characteristics (including coastal upwelling and water age) in controlling the rate and nature of surface carbon export. This is the latest in a suite of studies using Lagrangian frameworks to explain biological processes, including zooplankton hotspots (Messié & Chavez, 2017; Messié et al., 2022), diazotroph blooms triggered by

island mass effects (Messié et al., 2020), and the structure of plankton communities (Gangrade & Mangolte, 2024).

The satellite-based GA model shows significant promise in predicting carbon export and abyssal POC flux in the CCE, especially considering its high potential for improvement. One notable implication is that carbon export may be significantly more temporally variable than previously recognized. The research community is mostly looking to improve satellite algorithms by incorporating information on phytoplankton taxonomy provided by the newly launched PACE satellite (Cetinić et al., 2024; Kramer et al., 2024). Estimating export from coincident ocean color data may be adequate in stable, unproductive regions where phytoplankton and zooplankton are tightly coupled and horizontal advection is weak. However, in productive, dynamic regions such as the CCE, the accuracy of satellite-derived products is likely limited by spatiotemporal offsets between production and export. Explicitly incorporating the zooplankton contribution to export, including its offset from variables derived from ocean color, and oceanic advection, is a promising avenue to improve satellite-derived export products in the CCE and beyond.

Data Availability Statement

In situ data: CCE-LTER export data is available through the Environmental Data Initiative repository (California Current Ecosystem LTER et al., 2022). Station M abyssal POC time series is available on Zenodo (Huffard, 2024).

Satellite inputs: GlobCurrent is available online (E.U. Copernicus Marine Service Information, 2024). EF-OC is available online at https://spg-satdata.ucsd.edu/wc_productivity/wc_productivity.htm. The satellite-derived products used as inputs to Nsupply and GA were updated relative to Messié et al. (2022) (see Text S2 in Supporting Information S1); the updated Nsupply and Zbig monthly products are available on Zenodo (Messié, Sancho-Gallegos, et al., 2025) and updated monthly using near-realtime fields at https://www.mbari.org/data/nitrate-supply-estimates-in-upwelling-systems/ and https://www.mbari.org/data/krill-hotspots-in-the-california-current/, respectively.

Results: Daily GA export products ($C_{\text{production}}$ and export at a fixed 100 m depth) are available on Zenodo (Messié, Huffard, et al., 2025).

Software: Analyzes were performed using Matlab R2024a. The NPZ model is available on Zenodo (Messié, 2024) and https://github.com/messiem/toolbox_GrowthAdvection. The code to reproduce figures and main results from the paper is available at https://github.com/messiem/sourcecode_GAexport and published on Zenodo (Messié, 2025). Maps were displayed using m_map (Pawlowicz, 2020); the colorbar in Figure 1a is algae from *cmocean* (Thyng et al., 2016).

Acknowledgments
This research was funded by the David and Lucile Packard Foundation. The GA model was developed under a grant from the National Aeronautics and Space Administration (80NSSC17K0574). This research was also supported by National Science Foundation Grant OCE-2224726 to the CCE-LTER Program.

References

Baldwin, R., Glatts, R., & Smith, K. S., Jr. (1998). Particulate matter fluxes into the benthic boundary layer at a long time-series station in the abyssal NE Pacific. *Deep Sea Research Part II: Topical Studies in Oceanography*, *45*(4–5), 643–665. https://doi.org/10.1016/s0967-0645(97)00097-0

Blanke, B., & Raynaud, S. (1997). Kinematics of the Pacific equatorial undercurrent: An Eulerian and Lagrangian approach from GCM results. *Journal of Physical Oceanography*, *27*(6), 1038–1053. https://doi.org/10.1175/1520-0485(1997)027<1038:KOTPEU>2.0.CO;2

Bouffard, J., Vignudelli, S., Cipollini, P., & Ménard, Y. (2008). Exploiting the potential of an improved multimission altimetric data set over the coastal ocean. *Geophysical Research Letters*, *35*(10), L10601. https://doi.org/10.1029/2008GL033488

Brewin, R. J., Sathyendranath, S., Platt, T., Bouman, H., Ciavatta, S., Dall'Olmo, G., et al. (2021). Sensing the ocean biological carbon pump from space: A review of capabilities, concepts, research gaps and future developments. *Earth-Science Reviews*, *217*, 103604. https://doi.org/10.1016/j.earscirev.2021.103604

California Current Ecosystem LTER, Stukel, M., & Landry, M. (2022). Exported particulate carbon and nitrogen measurements from 4-day sediment trap deployments in the CCE region, 2007–2019 (ongoing) ver 7 [Dataset]. *Environmental Data Initiative*. https://doi.org/10.6073/pasta/cdee03ef7b17c2a4027a4a8b33c5b09b

Cetinić, I., Rousseaux, C. S., Carroll, I. T., Chase, A. P., Kramer, S. J., Werdell, P. J., et al. (2024). Phytoplankton composition from sPACE: Requirements, opportunities, and challenges. *Remote Sensing of Environment*, *302*, 113964. https://doi.org/10.1016/j.rse.2023.113964

Chabert, P., d'Ovidio, F., Echevin, V., Stukel, M. R., & Ohman, M. D. (2021). Cross-shore flow and implications for carbon export in the California current ecosystem: A Lagrangian analysis. *Journal of Geophysical Research: Oceans*, *126*(2), e2020JC016611. https://doi.org/10.1029/2020jc016611

Chavez, F. P., & Messié, M. (2009). A comparison of eastern boundary upwelling ecosystems. *Progress in Oceanography*, *83*(1–4), 80–96. https://doi.org/10.1016/j.pocean.2009.07.032

Cram, J. A., Weber, T., Leung, S. W., McDonnell, A. M. P., Liang, J., & Deutsch, C. (2018). The role of particle size, ballast, temperature, and oxygen in the sinking flux to the deep sea. *Global Biogeochemical Cycles*, *32*(5), 858–876. https://doi.org/10.1029/2017gb005710

DeVries, T. (2022). The ocean carbon cycle. *Annual Review of Environment and Resources*, *47*(1), 317–341. https://doi.org/10.1146/annurev-environ-120920-111307

Durkin, C. A., Cetinić, I., Estapa, M., Ljubešić, Z., Mucko, M., Neeley, A., & Omand, M. (2022). Tracing the path of carbon export in the ocean through DNA sequencing of individual sinking particles. *The ISME Journal*, *16*(8), 1896–1906. https://doi.org/10.1038/s41396-022-01239-2

E.U. Copernicus Marine Service Information. (2024). Global total (COPERNICUS-GLOBCURRENT), Ekman and geostrophic currents at the surface and 15m [Dataset]. *E.U. Copernicus Marine Service Information (CMEMS) Marine Data Store (MDS)*. https://doi.org/10.48670/mds-00327

Fiechter, J., Edwards, C. A., & Moore, A. M. (2018). Wind, circulation, and topographic effects on alongshore phytoplankton variability in the California Current. *Geophysical Research Letters*, *45*(7), 3238–3245. https://doi.org/10.1002/2017gl076839

Fiechter, J., Santora, J. A., Chavez, F., Northcott, D., & Messié, M. (2020). Krill hotspot formation and phenology in the California current ecosystem. *Geophysical Research Letters*, *47*(13), e2020GL088039. https://doi.org/10.1029/2020gl088039

Gangrade, S., & Mangolte, I. (2024). Patchiness of plankton communities at fronts explained by Lagrangian history of upwelled water parcels. *Limnology & Oceanography*, *69*(9), 2123–2137. https://doi.org/10.1002/lno.12654

Huffard, C. (2024). Fluxes of particulate organic carbon, nitrogen and mass from the Station M abyssal time series in the northeast Pacific, (1989–2022) [Dataset]. *Zenodo*. https://doi.org/10.5281/zenodo.14156812

Jönsson, B. F., Kulk, G., & Sathyendranath, S. (2023). Review of algorithms estimating export production from satellite derived properties. *Frontiers in Marine Science*, *10*. https://doi.org/10.3389/fmars.2023.1149938

Kahru, M., Goericke, R., Kelly, T. B., & Stukel, M. R. (2020). Satellite estimation of carbon export by sinking particles in the California Current calibrated with sediment trap data. *Deep Sea Research Part II: Topical Studies in Oceanography*, *173*, 104639. https://doi.org/10.1016/j.dsr2.2019.104639

Kramer, S. J., Jones, E. L., Estapa, M. L., Paul, N. L., Rynearson, T. A., Santoro, A. E., et al. (2024). Ocean carbon export can be predicted from ocean color-based phytoplankton communities. *bioRxiv*. (preprint). https://doi.org/10.1101/2024.09.21.613760

Kranz, S. A., Wang, S., Kelly, T. B., Stukel, M. R., Goericke, R., Landry, M. R., & Cassar, N. (2020). Lagrangian studies of marine production: A multimethod assessment of productivity relationships in the California current ecosystem upwelling region. *Journal of Geophysical Research: Oceans*, *125*(6), e2019JC015984. https://doi.org/10.1029/2019jc015984

Messié, M. (2024). Code for: Satellite-based Lagrangian model reveals how upwelling and oceanic circulation shape krill hotspots in the California Current System (v1.1.0) [Software]. *Zenodo*. https://doi.org/10.5281/zenodo.14144599

Messié, M. (2025). Code for: Spatial and temporal interplay between oceanic circulation and biological production in shaping carbon export off the California coast (v1.0.0) [Software]. *Zenodo*. https://doi.org/10.5281/zenodo.15022178

Messié, M., & Chavez, F. P. (2015). Seasonal regulation of primary production in eastern boundary upwelling systems. *Progress in Oceanography*, *134*, 1–18. https://doi.org/10.1016/j.pocean.2014.10.011

Messié, M., & Chavez, F. P. (2017). Nutrient supply, surface currents, and plankton dynamics predict zooplankton hotspots in coastal upwelling systems. *Geophysical Research Letters*, *44*(17), 8979–8986. https://doi.org/10.1002/2017GL074322

Messié, M., Huffard, C., Stukel, M., & Ruhl, H. (2025). Data from: Spatial and temporal interplay between oceanic circulation and biological production in shaping carbon export off the California coast (v1.0.0) [Dataset]. *Zenodo*. https://doi.org/10.5281/zenodo.14758969

Messié, M., Petrenko, A., Doglioli, A. M., Aldebert, C., Martinez, E., Koenig, G., et al. (2020). The delayed island mass effect: How islands can remotely trigger blooms in the oligotrophic ocean. *Geophysical Research Letters*, *47*(2), e2019GL085282. https://doi.org/10.1029/2019gl085282

Messié, M., Sancho-Gallegos, D. A., Fiechter, J., Santora, J. A., & Chavez, F. P. (2022). Satellite-based Lagrangian model reveals how upwelling and oceanic circulation shape krill hotspots in the California Current ecosystem. *Frontiers in Marine Science*, *9*(835813). https://doi.org/10.3389/fmars.2022.835813

Messié, M., Sancho-Gallegos, D. A., Fiechter, J., Santora, J. A., & Chavez, F. P. (2025). Data from: Satellite-based Lagrangian model reveals how upwelling and oceanic circulation shape krill hotspots in the California Current System [updated] (v2.1.0) [Dataset]. *Zenodo*. https://doi.org/10.5281/zenodo.14641977

Messié, M., Sherlock, R. E., Huffard, C. L., Pennington, J. T., Choy, C. A., Michisaki, R. P., et al. (2023). Coastal upwelling drives ecosystem temporal variability from the surface to the abyssal seafloor. *Proceedings of the National Academy of Sciences of the United States of America*, *120*(13), e2214567120. https://doi.org/10.1073/pnas.2214567120

Michaud, C. A., Huffard, C. L., Smith, K. L., & Durkin, C. A. (2022). Changes in phytoplankton and biomineral content of particles during episodic fluxes to abyssal depth. *Limnology and Oceanography Letters*, *7*(4), 342–353. https://doi.org/10.1002/lol2.10255

Nowicki, M., DeVries, T., & Siegel, D. A. (2022). Quantifying the carbon export and sequestration pathways of the ocean's biological carbon pump. *Global Biogeochemical Cycles*, *36*(3), e2021GB007083. https://doi.org/10.1029/2021gb007083

Pawlowicz, R. (2020). M_Map: A mapping package for MATLAB, version 1.4m [Software]. *EOAS*. Retrieved from www.eoas.ubc.ca/~rich/map.html

Pennington, J. T., Friederich, G. E., Castro, C. G., Collins, C. A., Evans, W. W., & Chavez, F. P. (2009). The northern and central California coastal upwelling system. In K.-K. Liu, L. Atkinson, R. Quiñones, & L. Talaue-McManus (Eds.), *Carbon and Nutrient Fluxes in Continental Margins. Global Change—The IGBP Series* (pp. 29–44). Springer-Verlag Berlin Heidelberg. https://doi.org/10.1007/978-3-540-92735-2_2

Picard, T., Baker, C. A., Gula, J., Fablet, R., Mémery, L., & Lampitt, R. (2024). Estimating the variability of deep ocean particle flux collected by sediment traps using satellite data and machine learning. *EGUsphere*. (preprint). https://doi.org/10.5194/egusphere-2024-3292

Plattner, G. K., Gruber, N., Frenzel, H., & McWilliams, J. C. (2005). Decoupling marine export production from new production. *Geophysical Research Letters*, *32*(11), L11612. https://doi.org/10.1029/2005GL022660

Pyper, B. J., & Peterman, R. M. (1998). Comparison of methods to account for autocorrelation in correlation analyses of fish data. *Canadian Journal of Fisheries and Aquatic Sciences*, *55*(9), 2127–2140. https://doi.org/10.1139/f98-104

Rio, M.-H., Mulet, S., & Picot, N. (2014). Beyond GOCE for the ocean circulation estimate: Synergetic use of altimetry, gravimetry, and in situ data provides new insight into geostrophic and Ekman currents. *Geophysical Research Letters*, *41*(24), 8918–8925. https://doi.org/10.1002/2014gl061773

Ruhl, H. A., Bahr, F. L., Henson, S. A., Hosking, W. B., Espinola, B., Kahru, M., et al. (2020). Understanding the remote influences of ocean weather on the episodic pulses of particulate organic carbon flux. *Deep Sea Research Part II: Topical Studies in Oceanography*, *173*, 104741. https://doi.org/10.1016/j.dsr2.2020.104741

Siegel, D. A., Buesseler, K. O., Doney, S. C., Sailley, S. F., Behrenfeld, M. J., & Boyd, P. W. (2014). Global assessment of ocean carbon export by combining satellite observations and food-web models. *Global Biogeochemical Cycles*, *28*(3), 181–196. https://doi.org/10.1002/2013GB004743

Siegel, D. A., DeVries, T., Cetinić, I., & Bisson, K. M. (2023). Quantifying the ocean's biological pump and its carbon cycle impacts on global scales. *Annual Review of Marine Science*, *15*(1), 329–356. https://doi.org/10.1146/annurev-marine-040722-115226

Smith, K., Jr., Huffard, C., & Ruhl, H. (2020). Thirty-year time series study at a station in the abyssal NE Pacific: An introduction. *Deep Sea Research Part II: Topical Studies in Oceanography*, *173*, 104764. https://doi.org/10.1016/j.dsr2.2020.104764

Smith, K. L., Jr., Ruhl, H. A., Huffard, C. L., Messié, M., & Kahru, M. (2018). Episodic organic carbon fluxes from surface ocean to abyssal depths during long-term monitoring in NE Pacific. *Proceedings of the National Academy of Sciences of the United States of America*, *115*(48), 12235–12240. https://doi.org/10.1073/pnas.1814559115

Smith, K. L., Jr., Ruhl, H. A., Kaufmann, R. S., & Kahru, M. (2008). Tracing abyssal food supply back to upper-ocean processes over a 17-year time series in the northeast Pacific. *Limnology & Oceanography*, *53*(6), 2655–2667. https://doi.org/10.4319/lo.2008.53.6.2655

Stephens, B. M., Durkin, C. A., Sharpe, G., Nguyen, T. T. H., Albers, J., Estapa, M. L., et al. (2024). Direct observations of microbial community succession on sinking marine particles. *The ISME Journal*, *18*(1), wrad010. https://doi.org/10.1093/ismejo/wrad010

Stukel, M. R., Décima, M., Kelly, T. B., Landry, M. R., Nodder, S. D., Ohman, M. D., et al. (2024). Relationships between plankton size spectra, net primary production, and the biological carbon pump. *Global Biogeochemical Cycles*, *38*(4), e2023GB007994. https://doi.org/10.1029/2023gb007994

Stukel, M. R., Irving, J. P., Kelly, T. B., Ohman, M. D., Fender, C. K., & Yingling, N. (2023). Carbon sequestration by multiple biological pump pathways in a coastal upwelling biome. *Nature Communications*, *14*, 2024. https://doi.org/10.1038/s41467-023-37771-8

Stukel, M. R., Kahru, M., Benitez-Nelson, C., Décima, M., Goericke, R., Landry, M. R., & Ohman, M. (2015). Using Lagrangian-based process studies to test satellite algorithms of vertical carbon flux in the eastern North Pacific Ocean. *Journal of Geophysical Research*, *120*(11), 7208–7222. https://doi.org/10.1002/2015JC011264

Stukel, M. R., Ohman, M. D., Benitez-Nelson, C. R., & Landry, M. R. (2013). Contributions of mesozooplankton to vertical carbon export in a coastal upwelling system. *Marine Ecology Progress Series*, *491*, 47–65. https://doi.org/10.3354/meps10453

Thyng, K., Greene, C., Hetland, R., Zimmerle, H., & DiMarco, S. (2016). True colors of oceanography: Guidelines for effective and accurate colormap selection. *Oceanography*, *29*(3), 9–13. https://doi.org/10.5670/oceanog.2016.66

References From the Supporting Information

Holte, J., Talley, L. D., Gilson, J., & Roemmich, D. (2017). An Argo mixed layer climatology and database. *Geophysical Research Letters*, *44*(11), 5618–5626. https://doi.org/10.1002/2017gl073426

Knauer, G. A., Martin, J. H., & Bruland, K. W. (1979). Fluxes of particulate carbon, nitrogen, and phosphorus in the upper water column of the northeast Pacific. *Deep-Sea Research, Part A: Oceanographic Research Papers*, *26*(1), 97–108. https://doi.org/10.1016/0198-0149(79)90089-x

Morel, A., Huot, Y., Gentili, B., Werdell, P. J., Hooker, S. B., & Franz, B. A. (2007). Examining the consistency of products derived from various ocean color sensors in open ocean (Case 1) waters in the perspective of a multi-sensor approach. *Remote Sensing of Environment*, *111*(1), 69–88. https://doi.org/10.1016/j.rse.2007.03.012

Rudnick, D. (2016). California underwater glider network [Dataset]. *Scripps Institution of Oceanography, Instrument Development Group*. https://doi.org/10.21238/S8SPRAY1618

Stukel, M. R., Kelly, T. B., Aluwihare, L. I., Barbeau, K. A., Goericke, R., Krause, J. W., et al. (2019). The Carbon:^{234}Thorium ratios of sinking particles in the California current ecosystem 1: Relationships with plankton ecosystem dynamics. *Marine Chemistry*, *212*, 1–15. https://doi.org/10.1016/j.marchem.2019.01.003